# International Journal of Mechanical Engineering Research and Technology

ISSN 2454-535X

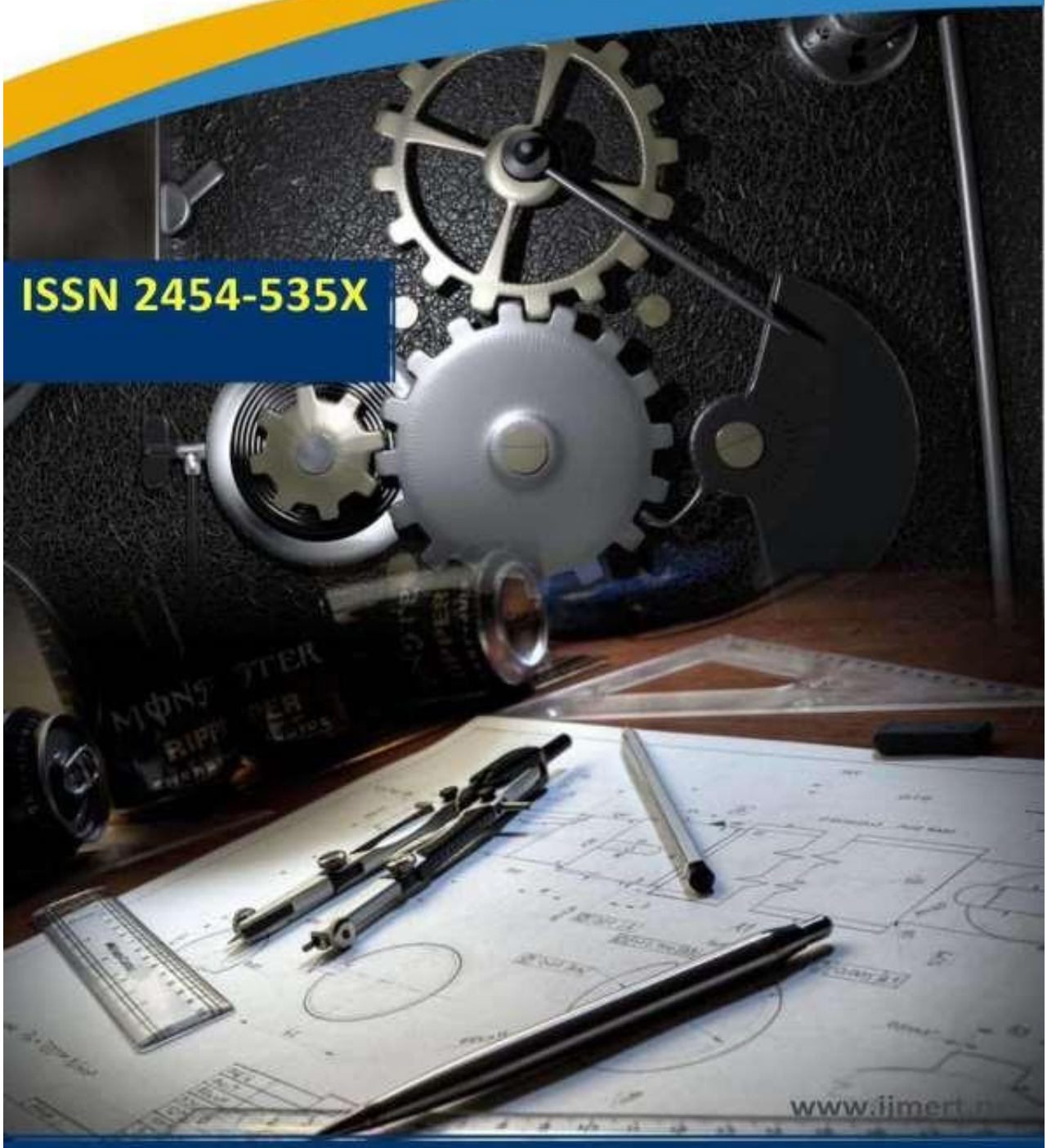

Email ID: info.ijmert@gmail.com or editor@ijmert.net

International Journal of Mechanical Engineering Research and Technology

ISSN 2454 – 535X
www.ijmert.com
Vol. 7 Issue. 2, may 2015

# Numerical Analysis of an Advanced Vapor Chamber-Heat Sink Design Embedded with PCM

**Swathi[1], Swetha[2] & Kalyani[3]**

[†]Electromechanical Eng. Department, University of Technology, Baghdad, Iraq

[‡]Department of Mechanical & Aerospace Engineering, University of Missouri, Columbia, USA.

*E-mail: 57hg@uotechnology.edu.iq

**ABSTRACT:**

As electrical appliances dissipate more heat now than ever before, effective cooling solutions are needed to address the high temperature issues that arise in several interior electrical device regions. This research provides a novel and sophisticated vapor chamber design that combines an enlarged surface area (fins) with a phase change material (PCM). The novel method uses copper foam and PCM-HS29P as a thermal storage, water as the working fluid, and pool boiling as the evaporation process. A numerical model and simulation study were carried out to remove 225W of heat generated from an electronic chip sized 2.5x2.5 cm2 and maintain the chip temperature below 70oC for a normal operation in order to explore the suggested design performance. The decision was made that when the new design

**KEYWORDS: Phase Change Material; Heat Sink; Cuckoo Search Technique, Heat Transfer, Numerical Analysis.**

## INTRODUCTION

As long as electronic companies continue to compete fiercely for technological leadership, there will be an increasing need for dependable, high-performing electronic components. As a result, upgrading is needed to meet the specifications for fast processing and chips with a high power density [1]. On the other hand, heat generation—a byproduct of electronic chip performance—is seen to be the primary obstacle impeding the advancement of technology in electronic equipment. The component temperature has an inverse relationship with the life expectancy and performance reliability of electronic equipment. Heat sinks, which are affixed to electronic components to increase surface area and transfer heat generation from the area where forced convective air cooling is occurring, are among the most widely used methods for cooling electronic chips.

## VAPOR CHAMBER WITH PCM

The conception being proposed here is to utilize the high capability of the PCMs as an additional heat storage which absorbs and releases heat when it melts and solidifies, respectively. In this design, the vapor chamber sides will be surrounded by the PCM which in turns will be connected to an extended surface area, fins. Figure 1 shows a schematic of the design concept. The vaporized working fluid at the base of the vapor chamber will exchange heat with the PCM and condense back to complete the circle.

Based on the thermodynamic principles, the highest heat dissipation occurs as the phase change is taking place. This amount of removal heat is equivalent to the latent heat of diffusion and solidification of the materials. Paraffin wax, metal hydrates, and fatty acids are examples of PCMs that can be used for latent thermal energy storage. However, during a phase change the temperature of the material remains constant means that a phase change process involves a large amount of heat transfer at a constant temperature; both are attractive features for heating, cooling, and temperature stabilization applications. According to that, using the PCMs in a sophistication amount will improve heat output absorption, keep the temperature constant, and enhance the safety of the vapor chamber design.

The main objective of this work is to demonstrate that the new approach has the capability to effectively and

International Journal of Mechanical Engineering Research and Technology
ISSN 2454 – 535X
www.ijmert.com
Vol. 7 Issue. 2, may 2015

safely maintain the temperature of an electronic chip under the design limit. Therefore, the proposed design will be tested under a case of study in which meets the needs of the developers of the electronic chips. Next coming sections will illustrate the design sections and analysis.

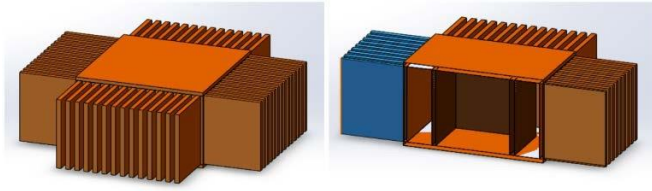

**Figure 1:** Schematic of the vapor chamber with PCM and fins

Design Characterizations

Due to its desirable thermal conductivity property, copper is the most likely choice to make the vapor chamber body and fins. However, this new vapor chamber has been approached without utilizing a wick structure, and that may effectively reduce the manufacturing cost of the whole system. Distilled water has been selected as a working fluid, and pool boiling evaporation progress is applied. Performance of the proposed design has been tested to remove 225W of heat generated from an electronic chip sized 1x1 in2, and maintain the chip temperature below 70oC for a normal operation. The geometrical parameters of the design are listed in Table 1and 2. The copper thickness of the vapor chamber frame and fins is 0.003m and 0.002m, respectively.

**Table 1.** Dimensions of the vapor chamber

| | Vapor Chamber | PCM Area | Fins |
|---|---|---|---|
| Length (m) | 0.06 | 0.06 | 0.06 |
| Width (m) | 0.06 | 0.02 | 0.05 |
| Height (m) | 0.06 | 0.06 | - |
| Gap (m) | - | - | 0.002 |
| Number of Fins | - | - | 14x4 |

For the thermal energy storage PCM, A promising composite material made of copper foam and PCM- HS29P is chosen. The ratio of Copper and PCM material is 50%. Copper foam is a product of Duocel® Copper Foam, which is already widely used in industry. PCM-HS29P is a product provided by RGEES LLC.It's uniquely engineered mixture of hydrated salts with high capacity to store thermal energy as latent heat. Itshows good thermal stability, thermal conductivity, and retain its latent heat without any change in physical

or chemical properties for over thousands of cycles [20]. Table 2. Shows the Properties of PCM-HS29P.

**Table 2.** Properties of the PCM-HS29P [20]

| Property | Value |
|---|---|
| Melting Temp. (°C) | 29 T |

International Journal of Mechanical Engineering Research and Technology
ISSN 2454 – 535X
www.ijmert.com
Vol. 7 Issue. 2, may 2015

| | |
|---|---|
| Freezing Temp (°C) | 29 T |
| Liquid Density (kg/m3) | 1550 |
| Solid Density (kg/m3) | 1840 |
| Latent Heat (kJ/kg) | 190 |
| Specific Heat-Liquid (kcal/kg·K) | 0.54 |
| Thermal Conductivity (W/m·K) Liquid | 0.54 |
| Thermal Conductivity (W/m·K) Solid | 1.09 |
| Base Material | CaCl2 |
| Congruent Melting | Yes |
| Sub Cooling | No |
| Flammability No - | No |
| | 5000 Internal |
| Thermal Stability (cycles) | |
| Max. Operating Temp (°C) | 80 |

The design will utilize a cooling fan to enhance heat dissipation. Heat transfer effectiveness, size, and noise output are the main concerns when choosing a fan. The heat sink demands 1.8 CFM of air flow from the fan. The fan must fit within the heat sink design; therefore, no frame dimension may exceed 25 mm. For comfortable operation, the fan should not exceed 30 dB. The ADDA AD2506fan from Shenzhen the Haixing and Electronics Company will be implemented in the design to meet all the requirements. Properties and specifications of the fan may be found in Table 3.

When using forced convection, or powered air flow, cooling is further enhanced by many heat sink characteristics. Ducting keeps the air flow in the heat sink and limits by-pass air. Fins should be oriented so as not to prevent air flow. The heat sink should be optimized for airflow and pressure drop so as not to put back pressure on the fan which could damage it. Lastly, wider heat sinks are usually more favorable than taller or longer designs.

**Table 3.** ADDA 25x25x10 mm DC Cooling Fan Specs. [21]

| Property | Value |
|---|---|
| Frame Size (mm) | 25x25x10 |
| Rated Voltage | 5V, 12 V |
| Rated Speed | 6,000~10,000 |
| Max Air Flow | 1.6~2.1 CFM |
| Max Noise | 18.5~23 dB |
| Life Expectancy (Ball Bearing) | 70,000 hrs |
| Life Expectancy (Hypro Bearing) | >5,000 hrs |
| Operation Temperature | -10~75 ºC |
| Storage Temperature | -40~75 ºC |

NUMERICAL ANALYSIS RESULTS

As prementioned in the design parameters, the input power of the chip, chip area, and vapor chamber area are 225W, 0.025x0.025 m2, and 0.06x0.06 m2, respectively. The heat flux can be found from

$q_{iin} \overline{\underline{Q}}_{\underline{Q}_{iin}A}1$

International Journal of Mechanical Engineering Research and Technology
ISSN 2454 – 535X
www.ijmert.com
Vol. 7 Issue. 2, may 2015

The following assumptions are made for the numerical analysis model:
$x = 0.06\,m.\ y = 0.02\,m.\ z = 0.06\,m.\ t = 0.003\,m.\ T_{air} = 293K = 20\,^oC$

Basic information of the base part and fins can also be found in Table 1. The heat transfer process might be characterized by a group of thermal resistances, shown in Figure 2, signifying heat charging and discharging modes as follows:
R1 - liquid-vapor phase change process resistance
R2 - vapor-condensate interfacial resistance
R3- condensate film resistance
R4 - column wall resistance (lateral direction)
R5 - PCM conduction resistance with foam
R6 - column wall resistance (lateral direction)
R7 - resistance of fin outside of PCM

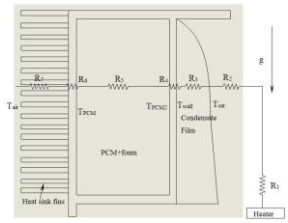


**Figure 2.** Thermal resistances network of the vapor chamber The number of fins is obtained as $N = \frac{Wb}{s+t_{ff}}$ The total volume of heat sink is (2)
$V_b = t_b x w_b x l_b$ (3)In order to enhance the heat transfer in fins, forced convection is added with certain fans or pumps. The ADDA DC cooling fan is recommended with a volume flow rate 1.8CFM, Table. 3, which equals to 8.4942
$\times 10^{-4}$ $m^3/s$. Thus, the air flow velocity is $v_a$ =8.4942$\times 10^{-4}$ $m^3$ /s ÷(0.01×0.01$m^2$)= 8.4942 m/s.

The correlated parameters are listed in Table 4. Except for the PCM foam part, the whole model is made of copper with thermal conductivity kwall =400W / (m.K).

**Table 4.** Parameters of air

| Property | Value |
|---|---|
| Thermal conductivity of air | $K_a$ = 0.0263W/(m.k) |
| Density of air (Kg/$m^3$) | ρ = 1.1614 kg/$m^3$ |
| Dynamic viscosity of air | μ = 184.6 x $10^{-7}$ N.s/$m^2$ |
| Prandtl number (Pr) | Pr = 0.707 |

Convectional heat transfer coefficient
Fins are cut into 10 sections in length to achieve a higher convection coefficient. So, the effective length of each fin is$l_{ba} = l_b/10$(4)
Reynolds number of the air flowing through gap is
$Re = \frac{\rho v_a l_{ba}}{\mu} = 3206.4 > 2300$(5)The corresponding Nusselt number is$Nu = 0.664\ Re^{1/2} Pr^{1/3}$ (6)The average convention coefficient acting on the fins is
$h_{ff} = \frac{k_a . l_{ba}}{} Nu$(The thermal resistance of the fin is obtained in the following process: the adjusted length of fins is$l_{ffffn} = l_{ff} + (\ _2)$(8)surface area of the base is$A_{sb} = (l_b * w_b) - (N * t_{ff} * l_b)$(9) perimeter of fins is$P = t_b + 2 * l_{ffn}$(10)cross sectional area of fins is$A_{cff} = t_{ff} * l_b$(11)surface area of the fin adjusted for adiabatic tip is

International Journal of Mechanical Engineering Research and Technology
ISSN 2454 – 535X
www.ijmert.com
Vol. 7 Issue. 2, may 2015

$A_{ff} = 2 * l_b * l_{ffn}$(12)total surface area of a fin surface array is
$A_t = N * A_{ff} + A_{sb}$(13)fin efficiency can be found

$$N_{ff} = \frac{\tanh}{} \quad (16)$$

$m_l$(1)Where$m_l = m *$
$l_{ffn}$(15)
and
$m = \sqrt{\frac{2P}{k_{wwall} * A_{cff}}}$
the overall efficiency is

$$N_o = 1 - \frac{N * A_{ff}}{A_t} * (1 - N_{ff})(17)$$

Finally, the thermal resistance of the overall fin array is
$R_7 = \frac{1}{N_0 * h_{ff} * A_t}$
(18)
Resistance of the base of the heat sink is
$R_6 = \frac{t_b}{k_{wwall} * (ww_b * l_b)}$
(19)
Temperature of the PCM is then achieved by
$T_{PCM} = T_{air} + \frac{Q_{iin}}{2} * (R_6 + R_7)$(20)

Then, the thermal resistance of the PCM foam is
$R_5 = \frac{y}{k_{PPPM} * x * z}$
(21)
Where, the thermal conductivity of the PCM foam is $k_{PCM} = 200.5\ WW/(m.K)$
Then, wall resistance is
$R_4 = \frac{t_{wwall}}{k_{wwall} * x * z}$
22)
The related temperature can be found:
$T_{PCM2} = T_{PCM} + q_{ii} * R_5 * x *$(23)
$T_{wwall} = T_{PCM} + q_{ii} * (R_4 + R_5) * x * z$(24)

In order to get thermal resistance of the liquid-vapor part in the chamber, assumption of $T_v$is needed
The first assumption is $T_v = 305K$; therefore, the relative parameters of water is $\rho_l = 993.7\ kg/m3$, $\rho_v = 0.0498\ kg/m3$, $k_l = 622.525\ WW/(m.K)$, then the saturation temperature can be obtained
$T_{sat} = T_{wwall} + R_3 * q_{ii} * x *$ (25) Then, the R3 and R2
are calculated as follow:

International Journal of Mechanical Engineering Research and Technology
ISSN 2454 – 535X
www.ijmert.com
Vol. 7 Issue. 2, may 2015

$$R_3 = \left(\frac{0.79 x_4 z_3 g \rho_{wwl}(\rho_{wwl}-\rho_{wwv}) k_{wwl}^3 h_{lv}}{\mu_l (T_{sat}-T_{wwall})}\right) \quad (26)$$

$$R_2 = \left[\left(\frac{2\rho.x.z}{2\rho}\right)\left(\frac{h_{lv}}{T_{sat} v_{lv}}\right)\left(\frac{M}{2\pi R_{uu} T_{sat}}\right)^{0.5}\left(1-\frac{P_{sat} v_{lv}}{2h_{lv}}\right)\right]^{-1} \quad (27)$$

Where, $Psat$ =5.6, M =1.8x10$^{-4}$, $\bar{R}$=8.31 J/mol.K

With the assumption, the real $T_v$ is found, if it's not different from the assumption, a new number is guessed for another iteration.

After finding the accurate number of $T_v$, the temperature of the chip can be found

$T_{boiil} = T_v + QQ_{iin} * R_2$(28)

$T_c = T_{boiil} + q_{iin}^{0.327}/C_1$(29)

Where, $T_{boiil}$ is the temperature due to pool boiling and the coefficient to get chip temperature is C1 = 2.5. Eq. 29 is derived from Stephan and Abdelsalam correlation of water $q'' = (C_1(T_{ww} - T_{sat(pl)}))^{1/0.327}$ in the nucleate region.

The boiling limitation is then examined by calculating the super heat of pool boiling

$dT = T_h - T_{boiil}$(30)

Numerical calculation results Results of the numerical model are listed in Table 5 below:

**Table 5.** Calculation results

| Property | Value |
|---|---|
| Heat flux | 62500W / m$^2$ |
| The number of fins | 15 |
| Total volume of heat sink | 1.08×10$^{-5}$m$^3$ |
| Effective length of each fin | 0.006m |
| Nusselt number | 33.4955 |
| Average convention coefficient | 146.8219W / (m$^2$ · K) |
| Adjusted length of fins | 0.051m |
| Surface area of base | 0.0018m$^2$ |
| Perimeter of fins | 0.105m |
| Cross sectional area of fins | 1.2×10$^{-4}$m$^2$ |
| Surface area of the fin adjusted for adiabatic tip | 0.0061m$^2$ |
| Total surface area of fin array | 0.0936m$^2$ |
| Fin efficiency | 0.9962 |
| Overall fin efficiency | 0.9963 |
| Temperature of PCM | 301.45K |
| Temperature of PCM inner side wall | 304.57K |
| Temperature of wall | 304.80K |
| Saturation temperature of water (phase change medium) | 305.97K |

International Journal of Mechanical Engineering Research and Technology
ISSN 2454 – 535X
www.ijmert.com
Vol. 7 Issue. 2, may 2015

| | |
|---|---|
| Temperature of pool boiling | 325.80K |
| Temperature of chip | 340.60K |

International Journal of Mechanical Engineering Research and Technology
ISSN 2454 – 535X
www.ijmert.com
Vol. 7 Issue. 2, may 2015

| | |
|---|---|
| Temperature difference (Superheat) | 14.80K |

The thermal resistances result of the numerical model are illustrated in Table 6. However, R1 has been neglected due to its small value which approximately considered zero.

**Table 6.** Numerical model thermal resistance results

| $R_{th}$ | Value |
|---|---|
| Resistance of the overall fin array | $R_7$ =0.0730W/(m$^2$·K) |
| Resistance of the base of the heat sink | $R_6$ =0.0021W/(m$^2$·K) |
| Thermal resistance of PCM foam | $R_5$ =0.0277W/(m$^2$·K) |
| Resistance of wall | $R_4$=□0.0021W/(m$^2$·K) |
| Condensate film resistance | $R_3$=□0.0104W/(m$^2$·K) |
| Vapor-condensate interfacial resistance | $R_2$ =0.0924W/(m$^2$·K) |

## RESULTS ANALYSIS

Conducting the numerical model showed promising results that focus on maintaining the chip temperature within normal working range and providing a safety factor for the overheating cases. Nevertheless, the results demonstrate the PCM role in chip protection by absorbing the unexpected heat. Figure 3 below, shows that when the vapor chamber heat sink outreaches 225W, the temperature of the chip is just 335.5K; it bellows the design required temperature 70oC (343K). Thus, the design is satisfied needs. However, as the heat output is continuously increasing, the chip temperature will keep evolving in a linear pattern. Therefore, the heat sink keeps on working to remove heat until the PCM material began melting. At this time, the output of the chip is already 275W and the chip is still below 70ºC, which is 68ºC. In conclusion, the proposal design meets the design requirement with a safety factor [22-25].

$$\eta\eta = \frac{275-225}{225} = 22\% \quad (31)$$

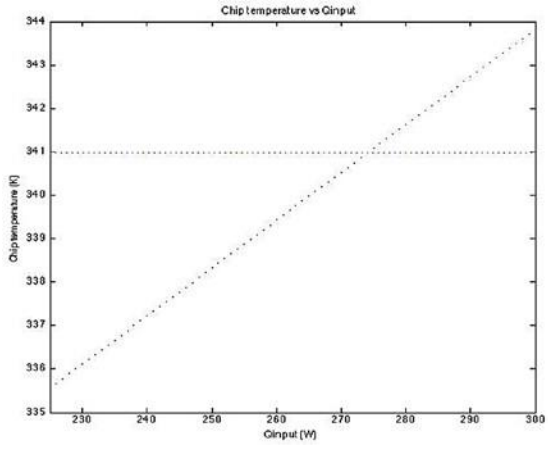


**Figure 3.** Chip temperature versus heat input

With this safety factor, the heat sink would keep the chip safety with a 50W more output. Figure 4 indicates that when the working out is 225W, the temperature of PCM material is just 300.7K, the melting temperature of PCM is 302K, the PCM would begin to melt when the output of the chip reaches 275W.

International Journal of Mechanical Engineering Research and Technology
ISSN 2454 – 535X
www.ijmert.com
Vol. 7 Issue. 2, may 2015

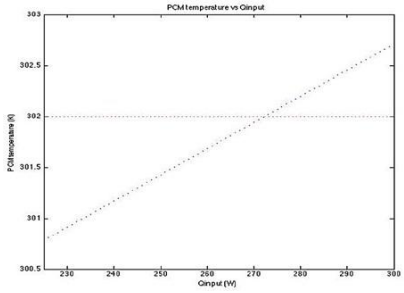


**Figure 4.** PCM temperature versus heat input

Figure 5 describes the time progress of the melting process of the PCM from solid to liquid phases. It takes 33 minutes to totally melting and become 100% liquid. Within the melting period, the PCM would keep changing phase and absorbing heat; the heat storage ability is 100kJ. Therefore, the temperature of the whole system will be invariant. For these 33 minutes, the chip would obviously be safe. Using PCM material is a key point of the design approach by adding extra protection to the chip from overheating.

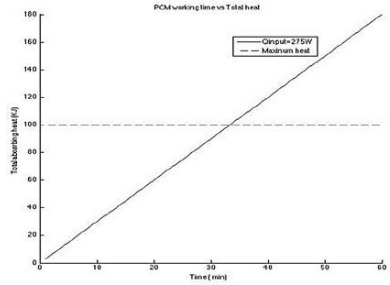


**Figure 5.** PCM working time of total melting

Figure 6 shows the pooling boiling limitation of this vapor chamber-heat sink. Since there is no an equation developed in other pressure, the equation used in the numerical analysis is pooling boiling equation in standard atmospheric pressure. Obviously, this figure illustrates that the superheat would increase as output is increased, but the difference is only 0.35K, which means superheat is mainly no change.

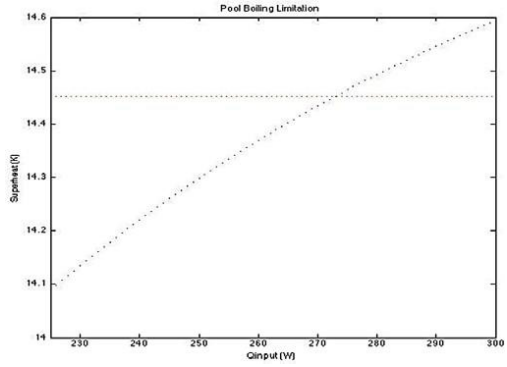

International Journal of Mechanical Engineering Research and Technology
ISSN 2454 – 535X
www.ijmert.com
Vol. 7 Issue. 2, may 2015

**Figure 6.** Pool boiling limitation versus heat input

For the numerical analysis process, thermophysical properties for saturated liquid and vapor are updated whenever Tv are changed in the process of iterative optimization because of varying other variables. Also, when the assumptions don't meet requirements of certain limitations, new numbers should be guessed and then iterate again. Thus, optimization is significantly important to get an accurate answer. An optimization flow- chart is shown in Figure 7.

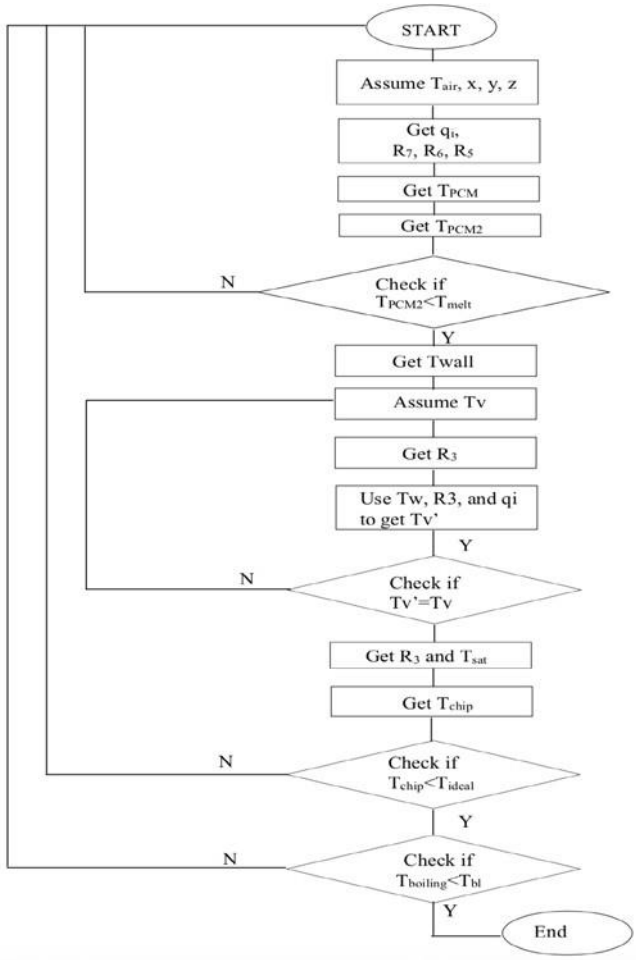


**Figure 7.** Optimization flow-chart of the vapor chamber-heat sink model

**Numerical simulation**

Heat transfer simulation was conducted by using ANSYS Steady State Thermal module. Comparing to analytical model, numerical model extends the numerical model into 3D. The pool boiling area is surroundedby PCM, and the whole structure is covered in the copper. The size is same as analytical model. Figure 8 is a section view of the whole structure. However, top cover in Figure 9 is suppressed to show the inner structure. Heat is added at the center of the bottom copper cover, with a total heat flow of 225W. Convection heat transfer isappliedatfoursidewallstoextractheatfromtheheatsink.

International Journal of Mechanical Engineering Research and Technology
ISSN 2454 – 535X
www.ijmert.com
Vol. 7 Issue. 2, may 2015

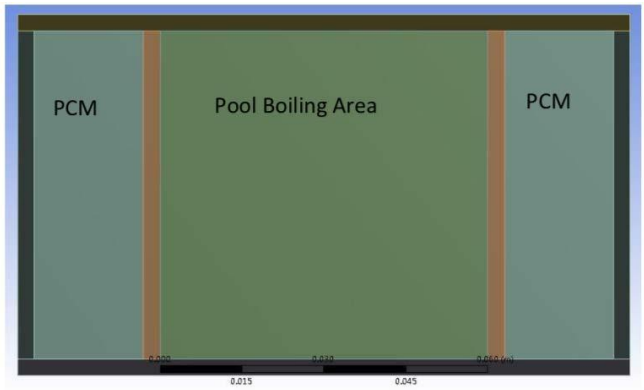


**Figure 8.** Section view for the vapor chamber-heat sink

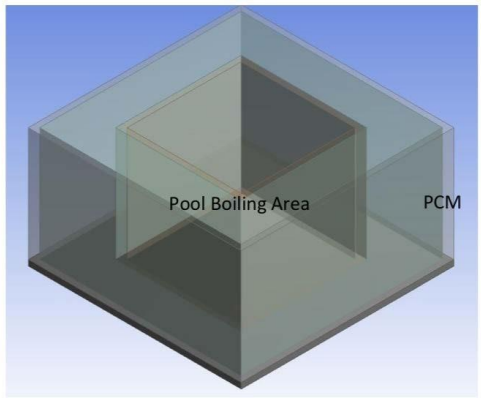


**Figure 9.** 3D view of the vapor chamber-heat sink

Several simplifications are made in this model:

1) Fin on the outer wall is ignored by increasing heat transfer coefficient using equation, so that temperature drop across the outer copper wall is the same as the one with fin on it. As in the analytical model.

$$h_{efff} = h_0 \frac{A_{ffiin}}{A_{efff}} \quad (32)$$

Where, $h_{efff}$ is effective heat transfer coefficient, $h_0$ is heat transfer coefficient with fin on the surface, $A_{ffiin}$ is surface area with fin, $A_{efff}$ is surface area without fin.

2) Pool boiling in the center of the structure is simulated by heat conduction, thermal conductivity is tuned to match the temperature difference from pool boiling and film condensation.

3) All interface resistance is ignored in this model, the value of contact thermal conductance is calculate using the smaller thermal conductivity of the two material in contact.

**Mesh dependency**

Three different meshes are used to test the grid dependency. Coarse mesh with 92182 nodes, 18619 elements; medium mesh with 261998 nodes, 55754elements; fine mesh with 515635 nodes, 113854 elements. The temperature result is listed in Table 7.

**Table 7.** Results of different meshes used

| Mesh Type | Maximum Temperature | Minimum Temperature |
|---|---|---|
| Coarse | 58.673 | 28.919 |
| Medium | 58.724 | 28.919 |

International Journal of Mechanical Engineering Research and Technology
ISSN 2454 – 535X
www.ijmert.com
Vol. 7 Issue. 2, may 2015

| | | |
|---|---|---|
| Fine | 58.698 | 28.919 |

Listed results demonstrate that comparing to fine mesh, the coarse mesh tends to underestimate the temperature, and the medium mesh tends to overestimate the temperature, but the difference between meshes is negligible, because the whole problem does not contain any transient or phase change problem. Analysis afterwards will base on the result from fine mesh.

**Temperature Result**

Figure 10 shows the temperature distribution inside the heat sink, this is the section view from the center of the heat sink, and we can see the heat is uniformly spread in the heat sink. Such a distribution is due to conduction assumption. The real temperature difference will concentrate at the bottom surface and side wall, which is the pool boiling area and film condensation area, Figure 11. With that kind of temperature distribution, it is expected that the heat transfer will be better compared to the numerical model; since pool boiling and film condensation will transfer heat more uniform from the chip to PCM.

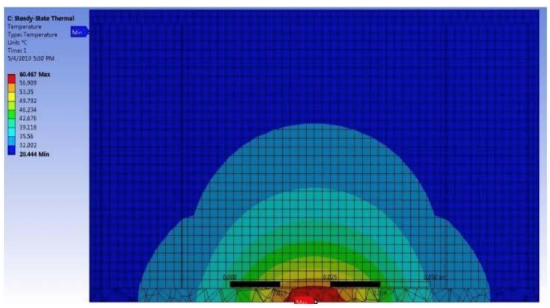

**Figure 10.** Section view of the temperature distribution inside the vapor chamber

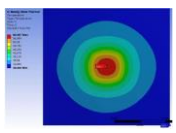

**Figure 11.** Bottom view of the vapor chamber temperature distribution

Figure 11 is the bottom temperature distribution. The figure is illustrated that the high temperature region is concentrate at the center of the bottom, where the power is added. Pool boiling in the real situation will spread the heat more uniformly to the side.

One very important temperature distribution is the temperature distribution in the effective phase change area. The effective thermal conductivity is determined by matching the temperature drop inside phase change section with the real temperature drop across the pool boiling area and film condensation area. Using this setup, the temperature difference in the phase change is 29 degree, which is similar to the numerical result; the temperature drops across the pool boiling area is 16 degree, and across film condensation is 9 degree, see Figure 12.

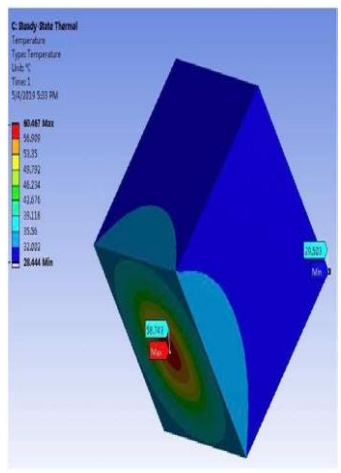

**Figure 12.** Temperature distribution within

International Journal of Mechanical Engineering Research and Technology
ISSN 2454 – 535X
www.ijmert.com
Vol. 7 Issue. 2, may 2015

the PCM

Figure 13 shows the temperature distribution in the PCM. Two labels on the figure show the highest and lowest temperature inside PCM. From the figure, the highest temperature is slightly lower than the melting temperature. However, the graphite foam greatly helped PCM to achieve a uniform temperature difference.

The numerical simulation model showed that the heat sink can keep the highest temperature on the chip under 70-degree Celsius and keep the highest temperature in PCM lower than the melting point. This simple numerical simulation is capable of extract 225W power from the chip.

The numerical now is a simplified model, no transient solution is provided in this model, a more accurate model can be created considering pool boiling and film wise condensation. However, due to the limited capability of ANSYS software on calculate melting and solidification, an effective liquid-vapor phase change may be practical to predict the heat transfer performance. User defined function (UDF) may be needed in order to describe the properties of the effective liquid-vapor phase change material.

**Figure 13.** Temperature distribution within the PCM

## CONCLUSION

A new advanced proposed vapor chamber design combined a phase change material (PCM) with fins is presented. A numerical model and simulation analysis were conducted. The new approach has shown that it is possible to have a heat sink with attractive features like high heat storage ability, fast charging ability, environment safe operation, high heat flux capability and high energy storage density including added features of a vapor chamber like self-acting and quiet operation. The promising aspects that make this concept feasible include using carbon foam in the thermal energy system columns (which help the thermal conductivity of heat to increase from 10.5 W/(m·K) to 205.5 W/(m·K), which helps in fast charging/heat absorption and a low heat flux at each column thus reducing the temperature gradients. Using of copper foam inside the PCM material of the chamber to ensure rapid transport of heat loads. With a safety factor 22% and heat storage ability 100kJ would give double assurance of the chip safety. Due to the absence of the wick structure fabrication in this design, the cost is reduced as long as the pool boiling is employed as evaporation progress.

## REFERENCES

[1] M. Fabbri, V.K. Dhir. “Optimized heat transfer for high power electronic cooling using arrays of microjets”. *Journal of heat transfer*, vol. 127, no. 7, pp. 760-769, 2005.

[2] S.P. Jang, S.J. Kim. “Fluid flow and thermal characteristics of a microchannel heat sink subject to an impinging air jet”. *Journal of heat transfer*, vol. 127, no. 7, pp. 770-779, 2005.

[3] Y. Koito, H. Imura, M. Mochizuki, Y. Saito, S. Torii. “Numerical analysis and experimental verification on thermal fluid phenomena in a vapor chamber”. *Applied Thermal Engineering*, vol. 26, no. 14-15, pp. 1669-1676, 2006.

[4] S.S. Hsieh, R.Y. Lee, J.C. Shyu, S.W. Chen. “Thermal performance of flat vapor chamber heat spreader”. *Energy Conversion and Management*, vol. 49, no. 6, pp. 1774-1784, 2008.

[5] Y.S. Chen, K.H. Chien, T.C. Hung, C.C. Wang, Y.M. Ferng, B.S. Pei. “Numerical simulation of a heat sink embedded with a vapor chamber and calculation of effective

International Journal of Mechanical Engineering Research and Technology
ISSN 2454 – 535X
www.ijmert.com
Vol. 7 Issue. 2, may 2015

thermal conductivity of a vapor chamber". *Applied Thermal Engineering*, vol. 29, no. 13, pp. 2655-2664, 2009.

[6] A. Gholami, M. Bahrami. "Thermal spreading resistance inside anisotropic plates with arbitrarily located hotspots". *Journal of Thermophysics and Heat Transfer*, vol. 28, no. 4, pp. 679-686, 2014.

[7] Y. Li, Z. Li, W. Zhou, Z. Zeng, Y. Yan, B. Li. "Experimental investigation of vapor chambers with different wick structures at various parameters". *Experimental Thermal and Fluid Science*, vol. 77, pp. 132-143, 2016.

[8] Y. Tang, L. Lin, S. Zhang, J. Zeng, K. Tang, G. Chen, W. Yuan. "Thermal management of high-power LEDs based on integrated heat sink with vapor chamber". *Energy conversion and management*, vol. 151, pp. 1-10, 2017.

[9] S.S. Hsieh, R.Y. Lee, J.C. Shyu, S.W. Chen. "Analytical solution of thermal resistance of vapor chamber heat sink with and without pillar". *Energy Conversion and Management*, vol. 48, no. 10, pp. 2708-2717, 2007.

[10] N. Ali, S. Ahmad, S. Aziz, G. Zaman. "The Adomian Decomposition Method for Solving HIV Infection Model of Latently Infected Cells". *Matrix Science Mathematic*, vol. 3, no. 1, pp. 05-08, 2019.

[11] E.C. Jekwu, A.G. Precious, A.B. Evans. "Evaluating the Impact of Unsteady Viscous Flow and Presence of Solid Particles on Pipeline Surfaces During Crude Oil Transport". *Acta Mechanica Malaysia*, vol. 2, no. 2, pp. 20-27, 2019. DOI: 10.26480/amm.02.2019.20.27

[12] S.H. Gian, S. Kasim, R. Hassan, Z. Zakaria, H. Mahdin, A.A. Ramli, M.F. Md Fudzee, M.A. Salamat. "Online Activity Duration Management System for Manufacturing Company". *Acta Electronica Malaysia*, vol. 3, no. 2, pp. 01-08, 2019.

[13] K.S. Shazwan, R. Shahari, C.N.A. Che Amri, N.S.M. Tajuddin. "Figs (Ficus Carica L.): Cultivation Method and Production Based in Malaysia". *Engineering Heritage Journal*, vol. 3, no. 2, pp. 6-8, 2019.

[14] J.S. Go. "Quantitative thermal performance evaluation of a cost-effective vapor chamber heat sink containing a metal-etched microwick structure for advanced microprocessor cooling". *Sensors and Actuators A: Physical*, vol. 121, no. 2, pp. 549-556, 2005.

International Journal of Mechanical Engineering Research and Technology
ISSN 2454 – 535X
www.ijmert.com
Vol. 7 Issue. 2, may 2015

[15] R. Boukhanouf, A. Haddad, M.T. North, C. Buffone. "Experimental investigation of a flat plate heat pipe performance using IR thermal imaging camera". *Applied Thermal Engineering*, vol. 26, no. 17-18, pp. 2148-2156, 2006.

[16] H.Y. Li, M.H. Chiang, C.I. Lee, W.J. Yang. "Thermal performance of plate-fin vapor chamber heat sinks". *International Communications in Heat and Mass Transfer*, vol. 37, no. 7, pp. 731-738, 2010.

[17] H.Y. Li, M.H. Chiang. "Effects of shield on thermal-fluid performance of vapor chamber heat sink". *International Journal of Heat and Mass Transfer*, vol. 54, no. 7-8, pp. 1410-1419, 2011.

[18] S. Wiriyasart, P. Naphon. "Thermal performance enhancement of vapor chamber by coating mini-channel heat sink with porous sintering media". *International Journal of Heat and Mass Transfer*, vol. 126, pp. 116-122, 2018.

[19] S. Wiriyasart, P. Naphon. "Fill ratio effects on vapor chamber thermal resistance with different configuration structures". *International Journal of Heat and Mass Transfer*, vol. 127, pp. 164-171, 2018.

[20] Y. Tang, L. Lin, S.W. Zhang, J. Zeng, K. Tang, G. Chen, W. Yuan. "Thermal management of high-power LEDs based on integrated heat sink with vapor chamber". *Energy Conversion and Management*, vol. 151, pp. 1-10, 2017.

[21] J. Velardo, A. Date, R. Singh, J. Nihill, A. Date, T.L. Phan, M. Takahashi, "Experimental investigation of a vapour chamber heat spreader with hybrid wick structure". *International Journal of Thermal Sciences*, vol. 140, pp. 28-35, 2019.

[22] M. Wang, W. Cui, Y. Hou. "Thermal spreading resistance of grooved vapor chamber heat spreader". *Applied Thermal Engineering*, vol. 153, pp. 361-368, 2019.

[23] V. Michels, F.H. Milanez, M.B. Mantelli. "Vapor chamber heat sink with hollow fins". *Journal of the Brazilian Society of Mechanical Sciences and Engineering*, vol. 34, no. 3, pp. 233-237, 2012.

[24] https://rgees.com/documents/aug_2013/savENRG%20PCM-HS29P.pdf

[25] http://www.pocographiteonline.com/servlet/Categories?category=Thermal